J. Fluid Mech. (1976), *vol.* 77, *part* 1, *pp.* 129–152
Printed in Great Britain

An approximate theory for incompressible viscous flow past two-dimensional bluff bodies in the intermediate Reynolds number regime $O(1) < Re < O(10^2)$

By SHELDON WEINBAUM, MICHAEL S. KOLANSKY, MICHAEL J. GLUCKMAN AND ROBERT PFEFFER
The City College of The City University of New York

(Received 8 April 1974 and in revised form 9 December 1975)

A new approximate theory is proposed for treating the flow past smoothly contoured two-dimensional bluff bodies in the intermediate Reynolds number range $O(1) < Re < O(10^2)$, where the displacement effect of the thick viscous layer near the surface of the body is large and a steady laminar wake is present. The theory is based on a new pressure hypothesis which enables one to take account of the displacement interaction and centrifugal effects in thick viscous layers using conventional first-order boundary-layer equations. The basic question asked is how the wall pressure gradient in ordinary boundary-layer theory must be modified if the pressure gradient along the displacement surface using the Prandtl pressure hypothesis is to be equal to the pressure gradient along this surface using a higher-order approximation to the Navier–Stokes equation in which centrifugal forces are considered. The inclusion of the normal pressure field with displacement interaction is shown to be equivalent to stretching the streamwise body co-ordinate in first-order boundary-layer theory such that the streamwise pressure gradient as a function of distance along the original and displacement body surfaces are equal.

While the new theory is of a non-rigorous nature, it yields results for the location of separation and detailed surface pressure and vorticity distribution which are in remarkably good agreement with the large body of available numerical Navier–Stokes solutions. A novel feature of the new boundary-value problem is the development of a simple but accurate approximate method for determining the inviscid flow past an arbitrary two-dimensional displacement body with its wake.

1. Introduction

Until very recently the development of approximate theoretical models for solving the Navier–Stokes equations for laminar flow have been limited to either very low Reynolds numbers, $Re < 1$, where inertia effects are either neglected or linearized, or very high Reynolds numbers, $10^3 < Re < 10^6$, where the simplifications of Prandtl's thin-boundary-layer theory are valid. Existing theoretical studies of flows in the intermediate Reynolds number range $1 < Re < 10^3$

have been confined primarily to numerical solutions of the full Navier–Stokes equations. These exact solutions, which provide an invaluable guide for the construction of approximate theoretical models, require large amounts of computer time on even the most advanced of the present generation of computers. The recent numerical studies of Gluckman (1971), Ghia & Davis (1974), Briley & McDonald (1974), Werle & Bernstein (1975) and Ghia, Ghia & Tesch (1975), however, strongly suggest that flows in the lower portion $O(1) < Re < O(10^2)$ of this intermediate Reynolds number range, where a steady laminar wake is observed on bluff bodies, can be analysed using boundary-layer-like models provided the viscous–inviscid displacement interaction with the external inviscid flow is adequately treated.

The present investigation proposes an approximate model, based on a new pressure hypothesis, which is able to predict to within a few per cent the location of separation and the detailed surface pressure and vorticity distribution on smoothly contoured semi-infinite and finite bodies. Detailed numerical comparisons with available two-dimensional finite-difference solutions of the Navier–Stokes equations for parabolas and circular cylinders are given. Equally good agreement with exact Navier–Stokes solutions for the axisymmetric flow past paraboloids of revolution and spheres is demonstrated in a companion paper, Kolansky *et al.* (1976).

Some idea of the magnitude of the displacement interaction on a bluff body at Reynolds numbers typical of those considered in the present study can be gleaned from the following example. At $Re = 30$ the displacement thickness at the forward stagnation point on a circular cylinder is about 15 % of its radius. At the location of separation, which is approximately 130° from the forward stagnation point for this Reynolds number, the displacement thickness has grown to about 0·7 radii and increases rapidly in the separated flow downstream. It is not surprising in view of the large changes in effective body shape which the external inviscid flow must experience at these Reynolds numbers that a theory of successive approximation which is based on the potential flow past the original body shape will converge very slowly. This would appear to be the basic difficulty encountered in extending the results of second-order boundary-layer theory (Van Dyke 1962) to flows with Reynolds numbers less than about 10^3.

In the past few years Davis, Ghia, Werle and co-workers have performed a series of numerical experiments, summarized in Ghia *et al.* (1975), that greatly elucidate the importance of the various terms in the Navier–Stokes equations in the Reynolds number range $O(1) < Re < O(10^3)$. In these numerical experiments several different approximate models of the complete two-dimensional Navier–Stokes equations are considered. In each model one solves an approximate viscous flow equation for the vorticity distribution throughout the entire flow field and a stream-function equation relating the vorticity ω to the two-dimensional stream function ψ. In the most accurate model, termed the parabolized-vorticity approximation (Ghia & Davis 1974), only the streamwise diffusion terms are dropped from the Navier–Stokes vorticity equation and the full elliptic stream-function equation is used. The results obtained are in almost perfect agreement with the exact Navier–Stokes solutions of Davis (1972) for

the flow past a parabola and of Ghia & Davis (1974) for the two-dimensional flow past a semi-infinite body with a shoulder, in which separation can occur depending on the shoulder bluntness. In a second model the curvature terms are omitted from the parabolized vorticity equation. The agreement with exact Navier–Stokes solutions is not quite as satisfactory as for the first model but still a significant improvement over that for conventional boundary-layer theory. In both these models the viscous–inviscid interaction describing the displacement and separation effects is automatically included since the full elliptic stream-function equation is used for the entire flow field. In a third model, called the parabolic approximation, the curvature terms are retained in the parabolic approximation to the Navier–Stokes vorticity equation, as in the first model, but a boundary-layer-like stream function is employed. Very good agreement with exact Navier–Stokes solutions could be obtained, except for cases of extreme shoulder curvature, provided that either the Navier–Stokes surface vorticity or the Navier–Stokes stream-function distribution in the inviscid external flow is prescribed. No difficulty is encountered in integrating through the separation-point singularity, confirming the result first reported by Catherall & Mangler (1966), that if the displacement interaction was properly accounted for, this singularity in the forward numerical integration of the boundary-layer equations could be removed. If, on the other hand, the Navier–Stokes interaction pressure or velocity field at the edge of the viscous layer was prescribed instead of the aforementioned vorticity or stream-function distribution, the difficulty in integrating through the separation point still persisted.

Further important evidence that the boundary-layer equations are still an adequate description of the development of the velocity profile in a thick viscous layer with strong displacement interaction is found in the work of Gluckman (1971) and Werle & Wornom (1972). These two studies show that, if either experimentally measured or Navier–Stokes surface pressure distributions are used to drive the Prandtl boundary-layer equations, good predictions of the location of the separation point and the surface vorticity distribution are possible for the flow past a circular cylinder for the entire range of Reynolds numbers where a steady wake separation bubble exists, even though all curvature effects have been omitted. These findings at first glance appear to contradict the results reported in Ghia *et al.* (1975), where curvature effects were shown to be important if close numerical agreement with the Navier–Stokes solutions was to be obtained. This can be explained if the curvature effects omitted from the boundary-layer equations themselves are retained in the description of the viscous layer as a modification of the surface pressure boundary condition. The results presented in this study provide strong evidence that this is indeed the case, since it is demonstrated that, if the streamwise co-ordinate along the body surface is stretched in accordance with the new pressure hypothesis derived herein, the pressure distribution along the surface of the body will agree remarkably well with the Navier–Stokes surface pressure distribution. The new pressure hypothesis states that if the conventional Prandtl boundary-layer equations are to include the lowest-order curvature effects in the viscous layer then the streamwise pressure gradient as a function of distance along the body surface should

be equal to the local pressure gradient as a function of distance along the displacement body. The hypothesis implies that the effective pressure interaction distance for a viscous layer with curvature using first-order boundary-layer equations is the streamwise distance measured along its centroid of vorticity. Lighthill (1958) has shown that this centroid is equivalent to the local displacement thickness of the viscous layer.

The crucial problem in the development of any approximate theory based on the matching of an inner viscous and outer inviscid flow is the construction of an effective displacement body when the inviscid pressure distribution used to determine the viscous-layer displacement growth is also unknown. In a matching problem of this nature one attempts to develop an iterative solution scheme based on a judicious initial guess of either the viscous-layer displacement growth or the inviscid pressure field. The same difficulty as caused the iterative solution procedure of second-order boundary-layer theory to break down at lower Re, the large distortion in effective body shape due to the displacement interaction of the thick viscous layers, however, can be used to advantage in a different scheme of successive approximation. For flows whose Reynolds numbers are $O(10^2)$ or less the details of the wake separation bubble on a bluff object such as a cylinder are completely enshrouded in the thick viscous layers that have developed along the body surface. As far as the inviscid outer flow is concerned, it is more important to approximate the qualitative shape and dimensions of the effective displacement body and its wake than the detailed geometry of the original body or the fine-structure of the separated flow region. To this end one seeks an iterative approximation procedure in which the lowest-order solution for the growth of the displacement thickness along the body surface already takes into account the change in surface pressure gradient due to the local enlargement of the body and centrifugal effects. The local inviscid pressure gradient obtained from a geometrically similar body whose local radius is equal to the local body radius plus the local displacement thickness provides a convenient geometry for generating the lowest-order solution. This simplified body approximately reproduces the local radius of curvature of the effective displacement body, the local flow characteristic which is of greatest importance according to the new pressure hypothesis stated above. The lowest-order approximation for the displacement body is now used to generate a new inviscid pressure distribution, which in turn is used to calculate a more accurate displacement-thickness distribution. The procedure is repeated until a converged solution of predetermined accuracy is obtained.

In § 2 we present the theoretical motivation behind the new pressure hypothesis. Section 3 states the boundary-value problems for the viscous and inviscid flow regions. The general solution procedure is outlined in § 4. Sections 5 and 6 describe the application of the new displacement interaction model to parabolic and circular cylinders and present detailed numerical comparisons with existing exact Navier–Stokes solutions for the flow past these bodies. Section 7 briefly discusses the results for other boundary shapes and concludes with some general comments about the validity and accuracy of the model.

2. The new pressure hypothesis for the viscous layer

In the conventional construction of the displacement body one refers the pressure along its surface back to the surface of the original body along the normal boundary-layer co-ordinate, treating the pressure as independent of this co-ordinate. This pressure mapping has implicit in it the assumption that the pressure gradient measured along the surfaces of the actual body and the displacement body are related by

$$\frac{dp}{ds_w} = \frac{R^*}{R_w}\frac{dp}{ds^*}, \tag{1}$$

where the subscript w denotes the wall, the superscript * the displacement body, s the distance along each surface and R the local radius of curvature assuming that both surfaces are nearly parallel. The difference in pressure gradient is thus $O(\delta)$ and is strictly a geometrical consequence of the wall curvature and is not related to the centripetal force field.

We now wish to examine how the streamwise pressure gradient varies across a thick viscous layer in which centrifugal effects are present to see how (1) must be modified to obtain a more accurate description of the wall pressure gradient. To this end we examine the following approximate set of governing equations for the viscous layer:

$$u\frac{\partial u}{\partial s} = -\frac{1}{\rho}\frac{\partial p}{\partial s} + \nu\frac{\partial^2 u}{\partial n^2}, \tag{2}$$

$$\frac{u^2}{R} = \frac{1}{\rho}\frac{\partial p}{\partial n}, \tag{3}$$

where s and n here refer to natural streamline co-ordinates. Note that the higher-order curvature correction for the viscous term in (2) has been omitted.

The simplifying feature of supersonic viscous–inviscid interaction theory is that there is a local relation between pressure and flow angle at the edge of the boundary layer. This simplification permits one to derive using rational asymptotic arguments the characteristic streamwise distance for a self-induced displacement interaction leading to separation and the characteristic thickness of the viscous sublayer near the wall. No equivalent rational theory has yet been developed for incompressible displacement interactions on bluff bodies leading to separation†. For high Reynolds number flow the size of the separated flow region is typically of the order of the body dimensions though the length of run for which the body boundary layer can withstand an adverse pressure gradient without separating is considerably shorter. For the thick viscous layers characteristic of the intermediate Reynolds number flows examined in the present study one observes that

† Recent theoretical studies of the displacement interaction at the trailing edge of a flat plate based on the asymptotic analyses of Stewartson (1969) and Messiter (1970) offer promise that such a rational theory can also be developed for bluff bodies at least in the limit of infinite Re. An intriguing feature of the asymptotic sharp trailing edge solution is that it agrees rather well with numerical Navier–Stokes solutions for Re in the range $O(1)$ to $O(10^2)$ considered herein. For bluff bodies one would not expect this agreement with an asymptotic analysis because of the important changes in effective wake shape as Re decreases.

the displacement thickness can double over a distance which is of the same order as the viscous layer's thickness. In accord with these remarks, we introduce the following dimensionless scaled co-ordinates into (2) and (3):

$$\tilde{R}' = \frac{R}{R_0}, \quad \tilde{n} = \frac{n}{\delta_0}, \quad \tilde{s} = \frac{s}{\delta_0}, \quad \tilde{u} = \frac{u}{U_\infty}, \quad \tilde{p} = \frac{p}{\rho U_\infty^2}. \tag{4}$$

Here $\delta_0 = Re^{-\frac{1}{2}} R_0$ is the characteristic thickness of the viscous layer and the Reynolds number is based on the body dimension R_0 and the free-stream velocity U_∞. Differentiating (3) with respect to s and substituting for $u\partial u/\partial s$ from (2) gives the following differential equation for the variation of the dimensionless streamwise pressure gradient across the viscous layer:

$$\frac{\partial}{\partial \tilde{n}}\left(\frac{\partial \tilde{p}}{\partial \tilde{s}}\right) + \frac{2}{Re^{\frac{1}{2}}\tilde{R}}\left(\frac{\partial \tilde{p}}{\partial \tilde{s}}\right) = -\frac{1}{Re^{\frac{1}{2}}}\left(\frac{\tilde{u}^2}{\tilde{R}^2}\right)\frac{\partial \tilde{R}_w}{\partial \tilde{s}} + \frac{2}{Re\,\tilde{R}}\frac{\partial^2 \tilde{u}}{\partial \tilde{n}^2}, \tag{5}$$

where the local radius of curvature is approximated by $\tilde{R} = \tilde{R}_w + Re^{-\frac{1}{2}}\tilde{n}$.

The integral of (5) which satisfies the condition

$$\partial \tilde{p}/\partial \tilde{s} = \partial \tilde{p}/\partial \tilde{s}_w \quad \text{at} \quad \tilde{n} = 0$$

is

$$\frac{\partial p}{\partial s} = \frac{\partial p}{\partial s_w}\left(\frac{R_w}{R}\right)^2 - \frac{1}{Re^{\frac{1}{2}}R^2}\left(\frac{\partial R_w}{\partial s_w}\right)\int_0^n u^2 dn + \frac{2}{Re\,R^2}\left(R\frac{\partial u(n)}{\partial n} - R_w\frac{\partial u(0)}{\partial n} - \frac{1}{Re^{\frac{1}{2}}}u(n)\right), \tag{6}$$

where the tildes have been dropped. Equation (6) relates the streamwise pressure gradient at any height n in the viscous layer to the wall pressure gradient $\partial p/\partial s_w$. The first term on the right-hand side of (6) represents the centrifugal correction due to the change in streamline curvature as one moves away from the wall. The second term represents the correction due to the streamwise change in curvature of the wall. This term vanishes for a circular cylinder and in general will be smaller than $O(Re^{-\frac{1}{2}})$ unless R_w changes to lowest order on a length scale $O(\delta_0)$. The quantities in parentheses in the third term constitute the viscous correction and are observed to be $O(Re^{-1})$ or smaller. The dominant correction to the streamwise pressure gradient as one moves away from the wall is thus seen to arise from the first term except in local regions with large changes in wall curvature, where the second term on the right-hand side of (6) will also be important. The viscous correction is of higher order in Re since the variation in the normal pressure field is principally due to centrifugal effects.

The important result which we wish to obtain from (6) is the relationship between the wall pressure gradient and the streamwise pressure gradient acting along the fictitious surface which the external flow perceives as the effective body shape including displacement effects. Denoting this effective displacement body by R^* and neglecting the higher-order viscous corrections, one finds from (6) that

$$\frac{\partial p}{\partial s^*} = \frac{\partial p}{\partial s_w}\left(\frac{R_w}{R^*}\right)^2 + \frac{1}{Re^{\frac{1}{2}}R^{*2}}\left(\frac{\partial R_w}{\partial s_w}\right)\int_0^{n^*} u^2 dn. \tag{7}$$

We now return to the original problem posed just prior to (2). The essential

question is whether (1), which is based on first-order boundary-layer theory and neglects all centrifugal effects, can be simply modified such that it generates a displacement body which has the same pressure distribution along its surface as that predicted by (7), which includes these effects. For the two pressure distributions to be equal to within an arbitrary constant one equates $\partial p/\partial s^*$ in (1) and (7). Denoting the wall pressure gradient predicted by (7) by the subscript n to signify the presence of the normal pressure field, one obtains

$$\frac{\partial p}{\partial s_{wn}} = \frac{dp}{ds_w}\left(\frac{R^*}{R_w}\right) - \frac{\partial R_w/\partial s_{wn}}{Re^{\frac{1}{2}} R_w^2}\int_0^{n^*} u^2\, dn. \tag{8}$$

For smoothly contoured bodies without rapid changes in surface curvature (8) reduces to

$$\frac{dp}{ds^*} = \frac{dp}{ds_w}, \quad ds_w = (R^*/R_w)\, ds_{wn} = ds^*. \tag{9}$$

Equation (9) states that the pressure gradient along the effective displacement body constructed in the conventional manner using first-order boundary-layer theory will be the same as in a viscous-layer theory which includes centrifugal forces provided the differential distance element ds_{wn} along the body surface is stretched by the factor R^*/R_w in mapping the pressure distribution from the displacement body back to the surface of the original body. This stretching implies that the pressure is referred from the displacement body back to the original body in a manner that preserves arc length, that is $ds_w = ds^*$.

The principal assumption introduced in the derivation of the new pressure hypothesis (8) or (9), is that the characteristic streamwise length scale for the displacement-induced viscous–inviscid interaction for a thick viscous layer is approximately $O(\delta_0)$. The assumption is based on numerical and experimental observations and not rational theoretical arguments. It is also assumed that the displacement surface is represented by a streamline in the viscous layer [see (7)] and that the local radius of curvature of the displacement body is equal to the local radius of curvature of the original body plus the local displacement thickness. Both assumptions are reasonable approximations at best. The derivation, despite its non-rigorous nature, leads to a result which greatly simplifies the treatment of curvature effects in thick viscous layers and provides remarkably good agreement with exact Navier–Stokes solutions.

In concluding this section we should mention that several other derivations of the pressure hypothesis have been tried. One approach that appeared particularly promising was based on the observation of Davis (1974) that the displacement body in the several flow geometries that he considered could be closely approximated by a conformal co-ordinate system. If this were the case then the flow past the displacement body could be transformed into a stagnation-point flow through a conformal mapping. As is well known the pressure gradient in a stagnation-point flow does not vary normal to the wall. This suggested that the streamwise pressure gradient might also exhibit special properties when its variation along the conformal co-ordinate normal to the displacement body was examined. One finds that for the flow past a wedge the normal derivative of the streamwise pressure gradient at the wedge surface vanishes but that this property is not in general true for other geometries.

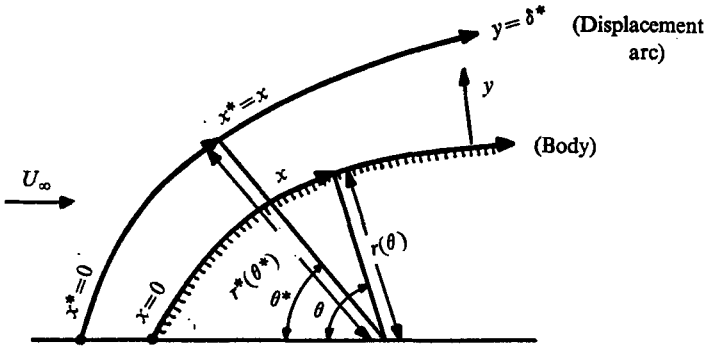

FIGURE 1. Boundary-layer co-ordinate system.

3. The new boundary-value problem

The new boundary-value problem for the matching of the inner viscous and outer inviscid flow fields differs from conventional theory principally in the construction of the effective displacement body and the application of the pressure hypothesis used to determine the wall pressure distribution. The governing equation for the viscous layer is the usual first-order boundary-layer equation

$$u\frac{\partial u}{\partial x}+v\frac{\partial u}{\partial y}=-\frac{1}{\rho}\frac{dp}{dx}+\nu\frac{\partial^2 u}{\partial y^2}. \tag{10}$$

Here x measures distance s_w along the original body surface and the pressure gradient is determined by the inviscid flow past the effective displacement body in accord with the pressure hypothesis (9). This hypothesis requires that

$$dp/dx = dp/dx^* \quad \text{with} \quad x = x^*, \tag{11}$$

where x^* is the distance s^* from the forward stagnation point of the displacement body. The pressure as a function of distance along the original body and the pressure as a function of distance along the displacement body are thus equal except for an additive constant due to viscous losses in total pressure along the streamline passing through the forward stagnation point. Since $r^* > r_w$ the local polar co-ordinate θ is stretched such that $\theta > \theta^*$ as shown in figure 1.

The effective displacement body is constructed by adding the displacement-thickness distribution

$$\delta^*(x)=\frac{1}{U(x)}\int_0^{\delta(x)}(U(x)-u)\,dy, \tag{12}$$

obtained from the solution of (10) for the velocity profile, to the original body surface. This construction differs from the conventional method of constructing the displacement body in that the inviscid pressure gradient at the position x^* (angular location θ^*) on the displacement surface is used to calculate the displacement thickness δ^* at the position x (angular location θ) on the original body in accord with the pressure mapping described by (11).

The inviscid pressure distribution and the velocity $U(x^*)$ at the surface of the displacement body are determined from the solution to the potential flow equation

$$\nabla^2\phi = 0 \tag{13}$$

for the velocity field. This solution satisfies the usual inviscid boundary condition that the normal component of the velocity vanishes at the displacement surface, i.e.

$$v(x^*) = 0 \quad \text{on} \quad r = r^*. \tag{14}$$

Since the solution for $\delta^*(x)$ depends on the solution for $U(x)$ and both are unknown, the solution of (10)–(14) represents a coupled nonlinear boundary-value problem. In essence, we wish to solve (13) subject to the known boundary condition (14) along an unknown surface, the effective displacement body. This body is determined from the solution of (10), in which the surface pressure distribution satisfies the pressure hypothesis (11) and must be obtained through a process of iterative approximation.

4. Solution procedure

The solution of the boundary-value problem just described to determine the effective displacement body requires that we make an initial guess of either the displacement-thickness distribution or the pressure distribution used in (10) to determine this distribution. The rapidity of convergence of the solution procedure depends in large measure on how good this initial estimate of δ^* or dp/dx is. For the reasons stated in the introductory section, it appears that the critical considerations in optimizing this first guess are the ability to reproduce the qualitative dimensions of the effective displacement body while taking account of the centrifugal effects in the thick viscous layer through the use of the new pressure hypothesis. An additional improvement in making this first guess can be obtained if at each step in the forward numerical integration of (10) the solution for the displacement-thickness distribution up to that step is somehow incorporated in the assumed expression for the local pressure gradient. To try to curve fit the displacement body accurately at each forward integration step would be extremely time consuming. A convenient practical expedient which uses the latest knowledge of the growth of the displacement body and provides improved numerical results is to represent the displacement body by a family of geometrically similar bodies whose local radius is the same as the local radius of the displacement body.

The above considerations were the important motivations behind the first trial solution for the displacement body that we have adopted. A summary of the complete solution procedure including the first trial solution is given below.

4.1. *First trial solution for the displacement body*

(1) Both the displacement thickness and the pressure gradient at the forward stagnation point are unknown. To approximate the displacement body a family of geometrically similar bodies with the same focal point as the original body is selected. The pressure or velocity gradient at the forward stagnation point on the displacement body is written in terms of the unknown displacement thickness and applied at the surface of the original body using the pressure stretching hypothesis (11). This expression is then solved simultaneously with (10) applied

at the forward stagnation point. The solution technique is illustrated in § 4.3 for the case of a circular cylinder.

(2) Having obtained this first trial solution for δ^*, dp/dx and the velocity profile at the forward stagnation point, one performs a forward numerical integration of (10). For present purposes it was deemed satisfactory to use the momentum integral approximation to (10) rather than the more accurate finite-difference solutions in view of the other approximations introduced. At each forward integration step the pressure gradient is represented by the local pressure gradient for the inviscid flow past the geometrically similar body whose local radius from the focal point of the original body is equal to that of the displacement body. From (11) this pressure gradient is also equal to the pressure gradient along the original body surface.

(3) The displacement-thickness distribution obtained from the solution described in step 2 is now added on normally to the surface of the original body. Because of the pressure mapping (11) the pressure gradient at the position x^* on the displacement body is used to calculate the displacement thickness at the position $x = x^*$ on the original body as shown in figure 1. This completes the first trial solution for the effective displacement body.

4.2. *The iteration procedure for a converged solution*

(1) As we shall observe in the results, the first trial solution just outlined provides a reasonable approximation to the displacement surface because it includes the streamwise co-ordinate straining required to describe curvature effects, but a poor detailed description of the surface pressure distribution since the actual shape of the displacement body and its wake can depart significantly from the family of geometrically similar bodies used in the first trial solution. The first step towards obtaining a converged solution is thus to obtain a much more accurate representation of the potential flow pressure distribution on the displacement body. This task is equivalent to solving (13) and (14) for an arbitrary boundary shape, since the displacement body obtained as in § 4.1 will not in general have a simple analytic representation. An approximate combined numerical and analytical solution technique based on the boundary method has been developed for this purpose and is described in § 4.4.

(2) The potential flow pressure distribution on the first-order displacement body obtained in step 1 above is now mapped back to the surface of the original body using (11). The momentum-integral-equation form of (10) is now solved again using this new pressure distribution.

(3) The new solution for the displacement-thickness distribution found in step 2 is now added on normally to the surface of the original body, in the same manner as before, to obtain the second-order approximation to the displacement body.

(4) Steps 1, 2 and 3 are now repeated to obtain the third- and higher-order approximations to the displacement body until convergence in either body shape or surface pressure distribution is achieved to within predetermined limits.

In accord with the preceding outline of the solution procedure, the approxi-

mate equation for the viscous layer is the integral of (10):

$$\frac{\tau_w}{\rho} = \frac{d}{dx}(U^2\theta) + \delta^* U \frac{dU}{dx}, \tag{15}$$

where τ_w is the wall shear and

$$\theta(x) = \int_0^\delta \frac{u}{U}\left(1-\frac{u}{U}\right) dy \tag{16}$$

is the momentum thickness. The velocity profile used is the Pohlhausen (1921) fourth-order polynomial profile

$$\frac{u}{U} = \left(2+\frac{\Lambda}{6}\right)\frac{y}{\delta} - \frac{\Lambda}{2}\left(\frac{y}{\delta}\right)^2 + \left(-2+\frac{\Lambda}{6}\right)\left(\frac{y}{\delta}\right)^3 + \left(1-\frac{\Lambda}{6}\right)\left(\frac{y}{\delta}\right)^4, \tag{17}$$

where the shape factor Λ is defined by

$$\Lambda = \frac{\delta^2}{\nu}\frac{dU}{dx}. \tag{18}$$

This profile provides a reasonable description up to separation and a solution of undetermined accuracy beyond the separation point. It is important to note that there is a marked difference between the velocity profiles of the separated flow in the present study and those at high *Re*, where there is a thin boundary-layer-like structure both in the reversed flow near the wall and in the separated free shear layers. The smoothly varying polynomial profile is much more likely to provide at least a qualitatively passable description of the separated thick viscous layers considered herein, where the spread of vorticity is much more diffuse.

4.3. *First trial solution for the forward stagnation point*

To elucidate the solution procedure described under step 1 in § 4.1, we consider the stagnation-point flow on a circular cylinder of unit radius. The geometrically similar displacement bodies considered are concentric cylinders of radius $r^* = 1+\delta^*$. Both δ^* and dU/dx at the forward stagnation point are unknown. The potential flow solution for the velocity on the surface of a geometrically similar displacement cylinder of radius r^* is

$$U = 2U_\infty \sin\theta^*, \tag{19}$$

where θ and θ^* are related by $\theta = r^*\theta^*$ from (11). The velocity gradient at the forward stagnation point on the original body surface obtained from (19) and the pressure transformation (11) is

$$dU/dx = 2U_\infty/(1+\delta^*). \tag{20}$$

It is well known that the solution of (15) at the forward stagnation point for a fourth-order Pohlhausen profile leads to a cubic equation for the shape factor Λ whose physically meaningful root is $\Lambda = 7{\cdot}052$, see Schlichting (1968, p. 197). The relationship between δ and δ^* for this profile is $\delta^* = \delta(\frac{3}{10} - \frac{1}{120}\Lambda)$. Substituting these last two results into (18) and (20) and eliminating dU/dx as an unknown, one obtains

$$\delta^{*2}/(1+\delta^*) = 1{\cdot}701/Re, \tag{21}$$

where Re is the free-stream Reynolds number based on the diameter of the original cylinder. The physically realizable solution for $\delta^*(0)$ is

$$\delta^*(0) = \frac{0{\cdot}856}{Re} + \left[\frac{1{\cdot}701}{Re} + \left(\frac{0{\cdot}856}{Re}\right)^2\right]^{\frac{1}{2}}. \tag{22}$$

It is interesting to observe that for $Re \gg 1$ equation (22) can be developed as a power series in inverse half-powers of the Reynolds number. This result,

$$\delta^*(0) = \frac{1{\cdot}304}{Re^{\frac{1}{2}}}\left(1 + \frac{0{\cdot}657}{Re^{\frac{1}{2}}} + \frac{0{\cdot}213}{Re} + \ldots\right), \tag{23}$$

is of the same form as one would anticipate from higher-order boundary-layer theory. The leading term in (23) is the same as the one obtained from the solution for a two-dimensional stagnation point while the higher-order terms are due to viscous-layer displacement and curvature effects.

The solution procedure for other boundary shapes differs only in the expression for the surface velocity distribution (19).

4.4. *Inviscid flow past the displacement body*

The crucial step in the iterative approximation procedure used to obtain a converged solution is the development of a simple yet accurate approximate technique for determining the flow past non-analytic boundary shapes. In theory the exact solution for the two-dimensional streaming motion past an arbitrary cylinder can be represented by an appropriate surface distribution of line sources and sinks. Accurate approximate representations for smoothly contoured bodies can be obtained using internal source–sink distributions by applying the boundary method. The detailed application of the boundary method developed herein differs depending on whether the body is of low or high aspect ratio. In either case one starts with an unknown finite distribution of N sources and sinks of strength m_i located at positions x_i along the plane of symmetry of the body and placed in a uniform stream. The stream function for this flow,

$$\psi = U_\infty y + \sum_{i=1}^{N} m_i \left(\tan^{-1}\left(\frac{y}{x - x_i}\right) - \pi\right), \tag{24}$$

automatically satisfies (13). Far upstream of the body each term in the finite series vanishes and (24) reduces to the stream function for a uniform stream. Far downstream the $\psi = 0$ streamline, representing the displacement body, asymptotically approaches a far wake of uniform thickness d determined by the net source strength:

$$d = \frac{\pi}{U_\infty} \sum_{i=1}^{N} m_i. \tag{25}$$

The essential feature of the present application of the boundary method is that one wishes to satisfy the boundary conditions (14) along the arc of the displacement body through judicious selection of the unknown constants x_i and m_i. This is accomplished by setting $\psi = 0$ in (24) at discrete points along the displacement surface $r^*(x^*)$. The arbitrariness of the method lies in the selection of the boundary points and the choice as to which values of x_i and m_i one wishes

to leave unspecified. After considerable numerical experimentation two different procedures have been adopted in the present study. For the flow past finite bodies of low and moderate aspect ratio, such as the circular cylinder and ellipses treated herein, it was observed that a surprisingly good representation of the desired $\psi = 0$ boundary shape could be obtained using only four equally spaced boundary points between flow attachment and separation if both m_i and x_i were left unspecified and the series in (24) was truncated at $N = 2$. A typical curve fit is discussed later in figure 4. The unusually good agreement obtained using only two source–sink singularities can be attributed to the smoothly varying contour of the displacement body and the fact that the detailed geometry of the wake downstream of the body is not important as far as the surface pressure distribution is concerned, and thus does not have to be accurately modelled.

For the flow past semi-infinite bodies, such as the family of parabolas considered herein or finite bodies of high aspect ratio, many more boundary points are required for an accurate curve fit in which the $\psi = 0$ streamline does not exhibit wave-like undulations. The solution of the matrix of equations derived from (24) when many boundary points are required is extremely tedious if both m_i and x_i are treated as unknowns since the x_i appear nonlinearly as the arguments of the inverse tangents. A much simpler procedure for these extended bodies is to specify the source–sink locations x_i and leave only the values of m_i to be determined since these constants appear linearly in (24). A convenient but arbitrary selection of boundary points and source locations in this procedure is to position the singularities directly below the boundary points in one-to-one correspondence. Employing standard matrix reduction schemes for systems of linear equations, one can easily handle as many as 100 boundary points using less than a second of computer time.

5. Parabolic cylinders

As the first application of the new approximate theory described in §§ 3 and 4, we consider the uniform viscous flow past a parabolic cylinder whose surface is defined by

$$y^2 = 4(1+x) \tag{26}$$

at various Reynolds numbers. This simple body shape, for which separation does not occur, provides a convenient geometry to test the basic hypotheses of the new model with existing finite-difference solutions of the Navier–Stokes equations (Davis 1972) and conventional boundary-layer theory.

The family of geometrically similar parabolas used to generate the surface pressure distribution in (15) for the construction of the first trial guess for the displacement body is given by

$$y^2 = 4c^2(x+c^2). \tag{27}$$

For $c = 1$ this reduces to (26) whereas for $c > 1$ one obtains a family of geometrically enlarged parabolas with a common focal point at the origin.

The transformation $w = u+iv$, where

$$w = -z^{\frac{1}{2}} + ic, \tag{28}$$

maps the flow past the parabolic surfaces described by (27) in the complex z plane into a two-dimensional stagnation-point flow in the complex w plane, the parabolic surfaces mapping into the v axis. The solution for the complex potential $F(w) = \phi + i\psi$ in the transformed w plane is $F(w) = U_\infty w^2$. Differentiating this result, one obtains for the speed q in the z plane

$$q = |F'(z)| = U_\infty \left[1 + \frac{c^2}{r} - \frac{2c}{r^{\frac{1}{2}}} \sin\left(\frac{\pi - \theta^*}{2}\right)\right]^{\frac{1}{2}}, \tag{29}$$

where the angle θ^* is measured from the forward stagnation point. From (29) the speed along the surface of the parabolas defined by (27) is

$$q = U = U_\infty \cos \tfrac{1}{2}(\pi - \theta^*). \tag{30}$$

The potential flow solution (30) replaces (19) in the first trial solution for the flow at the forward stagnation point and is also used to approximate the local pressure gradient in (10) or (15) as described in step 2 in § 4.1. In applying the pressure mapping described by (11) we have related the polar angles θ and θ^* measured from the forward stagnation point along the original and effective displacement body surfaces by the arc-length formula

$$\int_0^{\theta^*} \left[r^{*2} + \left(\frac{dr^*}{d\theta}\right)^2\right]^{\frac{1}{2}} d\theta = \int_0^{\theta} \left[r^2 + \left(\frac{dr}{d\theta}\right)^2\right]^{\frac{1}{2}} d\theta. \tag{31}$$

In the discussion beneath (11) it was mentioned that the pressure distributions as functions of distance along the original and displacement surfaces respectively are equal to within an additive constant due to the viscous loss in total pressure along the stagnation streamline. To determine this constant we consider the two-dimensional Navier–Stokes equation in the vicinity of the stagnation point. In this region the normal velocity component is independent of x and the normal momentum equation reduces to

$$v \frac{dv}{dy} = -\frac{1}{\rho}\frac{\partial p}{\partial y} + \nu \frac{\partial^2 v}{\partial y^2}. \tag{32}$$

The integral of (32) between the wall and the edge of the viscous layer, denoted by the subscript e, is

$$\tfrac{1}{2} v_e^2 = -\rho^{-1}(P_e - P_w) - \nu \, \partial v_e / \partial y. \tag{33}$$

Combining this result with the Bernoulli equation applied along the stagnation streamline in the inviscid flow, one obtains the following expression for the increase in wall pressure coefficient due to viscous losses:

$$C_{pw} = \frac{P_w - P_\infty}{\rho U_\infty^2} = \frac{1}{2}\left(1 + \frac{4}{Re}\frac{\partial v_e}{\partial y}\right). \tag{34}$$

The Reynolds number here is based on the radius of curvature R_0 at the forward stagnation point. For a parabola this is equal to twice the focal radius.

In figures 2 (a) and (b) we have compared the results of the present approximate model with the numerical Navier–Stokes solutions of Davis (1972) for the surface pressure distribution on a parabola at a Reynolds number of 10 and 100. The importance of the viscous pressure losses predicted by (34) and the streamwise stretching of the body surface co-ordinate required by the pressure hypothesis (11) is particularly evident for the $Re = 10$ flow. The potential flow pressure

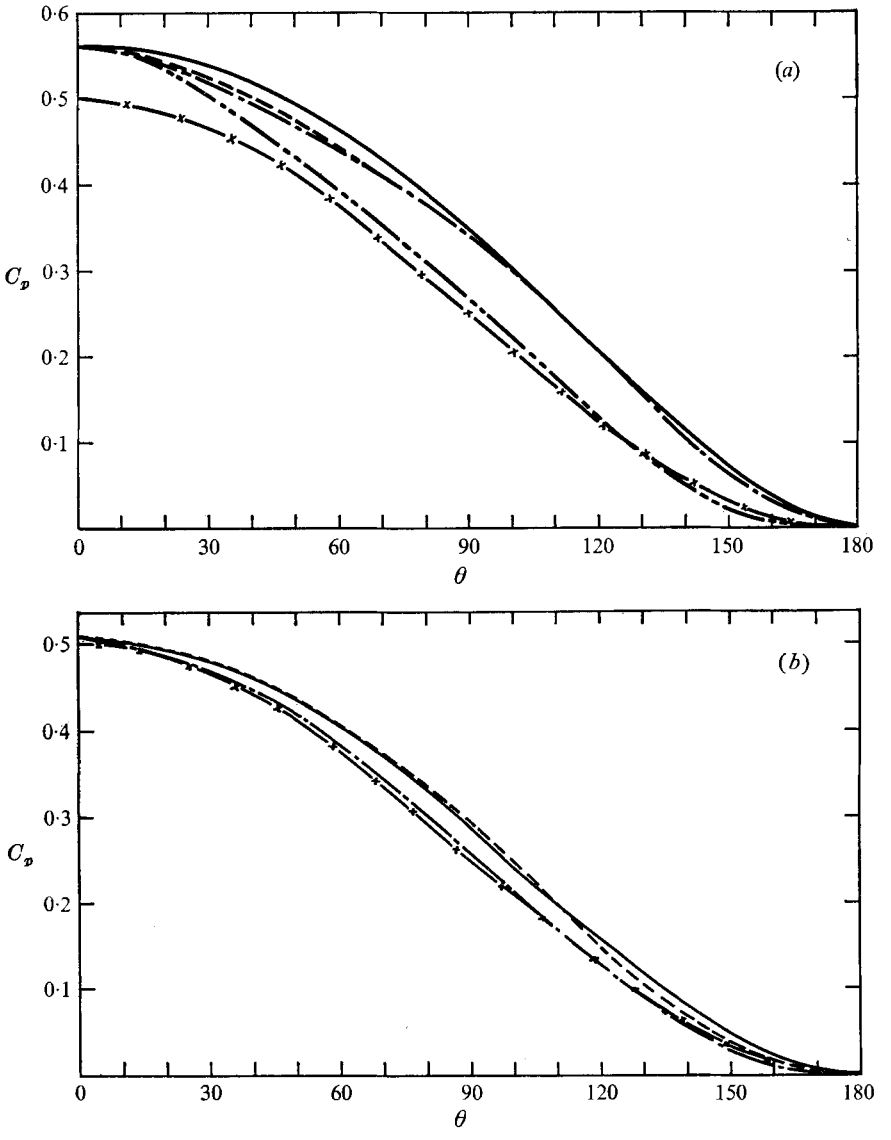

FIGURE 2. Surface pressure distribution for a parabolic cylinder. (*a*) $Re_\infty = 10$. ——, Davis (1972); — · —, first-order approximation; – – –, second-order approximation; — · · —, second-order boundary-layer theory; — × —, inviscid. (*b*) $Re_\infty = 100$. ——, Davis (1972); – – –, first-order approximation; — · —, second-order boundary-layer theory; — × —, inviscid.

distribution for the inviscid flow past the original body considerably lags the Navier–Stokes solution for the surface pressure over the entire body. The inclusion of viscous-layer displacement effects using conventional first-order boundary-layer theory to construct the displacement body and no stretching yields a curve (not shown) which is almost identical on the scale shown to the potential flow past the original parabola, while the inclusion of the viscous pressure losses from (34) serves only to elevate the surface pressure distribu-

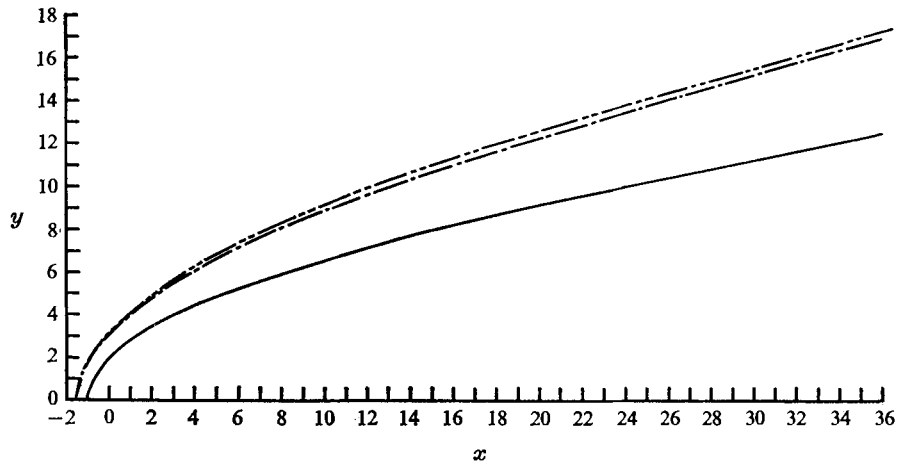

FIGURE 3. Stream-function fit of the displacement body for a parabolic cylinder. $Re_\infty = 10$. ———, original body, $y = 4(1+x)$; — · —, second-order displacement body; — - - —, second-order boundary-layer theory.

tion in the forward stagnation region. A very substantial improvement in the agreement with the exact Navier–Stokes solutions is achieved, however, with both the first- and second-order approximations to the displacement body using the new pressure stretching hypothesis and the viscous correction for the pressure loss across the layer. The first-order approximation is based on the family of geometrically similar parabolas (27), the pressure gradient being mapped back to the body surface in accord with (31). The second-order approximation is based on a stream-function fit of (24) to the first-order approximation for the displacement body. A typical curve fit employing 25 boundary points is able to generate a $\psi = 0$ boundary streamline which is nearly indistinguishable from the desired shape.

At first glance the very close agreement between the first- and second-order approximate solutions for the surface pressure distribution in figure 2(*a*) might seem surprising in view of the substantially different manner in which they were calculated. The reason for this close agreement is evident from figure 3, where we have plotted the stream-function fit to the second-order displacement body. The first- and second-order displacement bodies are almost identical; one therefore concludes that the displacement-thickness distribution predicted by the potential flow past the geometrically similar family of parabolas is nearly the same as that predicted by (24). Also shown in the figure is the second-order displacement body obtained when the integral equation (15) for the viscous layer is solved using the potential flow past the original body and the displacement body constructed in the conventional manner.

6. Circular cylinders

A much more rigorous test of the new approximate theory is the flow past a circular cylinder in the Reynolds number range 5 to approximately 60, where a

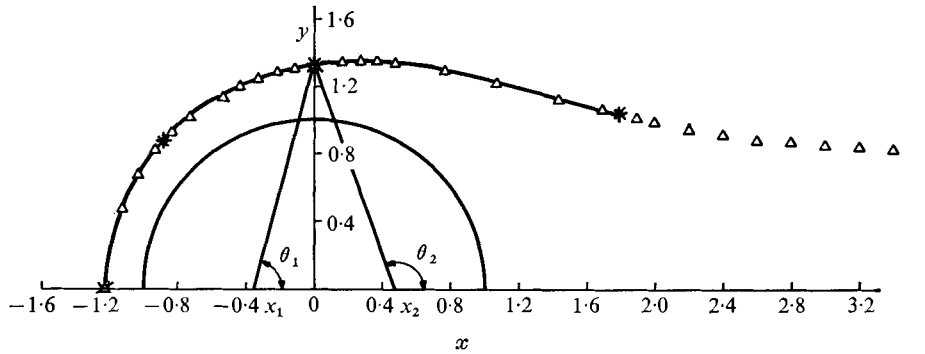

FIGURE 4. Stream-function fit of the displacement body for a circular cylinder. $Re_\infty = 10$. ———, first-order approximation; △, stream-function fit; ✱, match points.

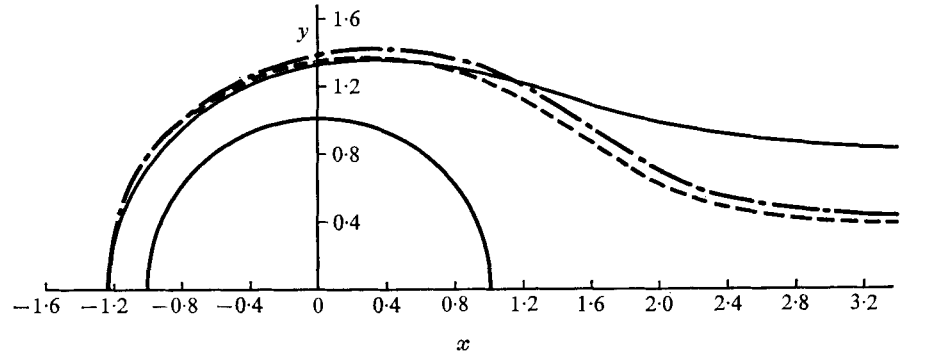

FIGURE 5. Successive approximations for the displacement body for a circular cylinder. $Re_\infty = 10$. ———, first-order approximation; —·—, second-order approximation; – – –, third-order approximation.

closed steady wake separation bubble is observed in both experiments and numerical Navier–Stokes solutions.

The solution scheme for circular cylinders has already been described in detail in §4. Equation (15) when integrated using the surface velocity distribution (19) yields the first trial solution for the displacement body. This body, for a Reynolds number of 10, is illustrated in figure 4. Also shown in this figure is the approximate solution for the inviscid flow past this displacement body obtained using (24) with $N = 2$, as discussed in §4.4. The four march points used are denoted by asterisks. The last asterisk denotes the point of separation. The stream-function fit, which has been continued past the point of separation, approaches the asymptotic wake width predicted by (25). The surprisingly good approximation that can be obtained for the displacement body using only two source–sink singularities is clearly evident in this figure.

Figure 5 shows the displacement bodies obtained by the iteration procedure described in §4.2. The significant deviation between the first- and higher-order approximations arises because the second- and higher-order approximations predict separation at a smaller angle ϕ from the rear stagnation point. This is shown in figure 6, where we have compared the theoretically predicted location

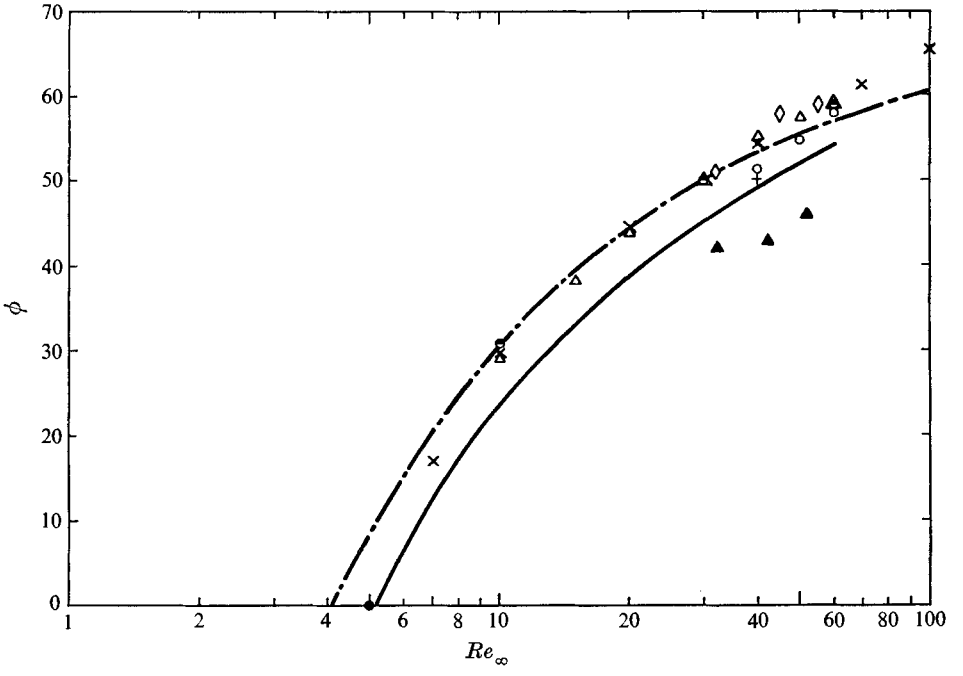

FIGURE 6. Separation angle as a function of Reynolds number for a circular cylinder. —·—, first-order approximation; ———, second-order approximation; △, Takami & Keller (1969); ◑, Kawaguti & Jain (1966); ○, Jain & Rao (1969); +, Apelt (1961); ▲, Grove *et al.* (1963); ◇, Homann (1936); ●, Taneda (1956); ×, Dennis & Chang (1970).

of separation as a function of Reynolds number with available experimental data and Navier–Stokes solutions. The present first-order approximation provides slightly better agreement than the second- and higher-order approximations at the higher Reynolds numbers, whereas the latter nearly exactly predict Taneda's (1956) experimentally observed Reynolds number for incipient separation. The difference between second- and higher-order approximate solutions is in general very small, as observed in figure 5.

The crucial test of the new theory is whether it can accurately predict the surface pressure distribution on the cylinder. Figures 7(*a*)–(*c*) illustrate the excellent results obtained using the new pressure hypothesis equation (9) or (11). Also shown in these figures is the surface pressure predicted by standard second-order boundary-layer theory using the conventional construction of the displacement body. In the present study we have been primarily concerned with determining the surface pressure up to the point of separation, since the fourth-order polynomial profile description given by (17) is a poor detailed representation of the flow in the separated flow region. The pressure at the rear stagnation point on the cylinder could, therefore, not be used as the zero reference value as is commonly done in the numerical Navier–Stokes solutions. Instead we have chosen the pressure at the forward stagnation point predicted by numerical Navier–Stokes solutions as the reference pressure for all the circular-cylinder calculations.

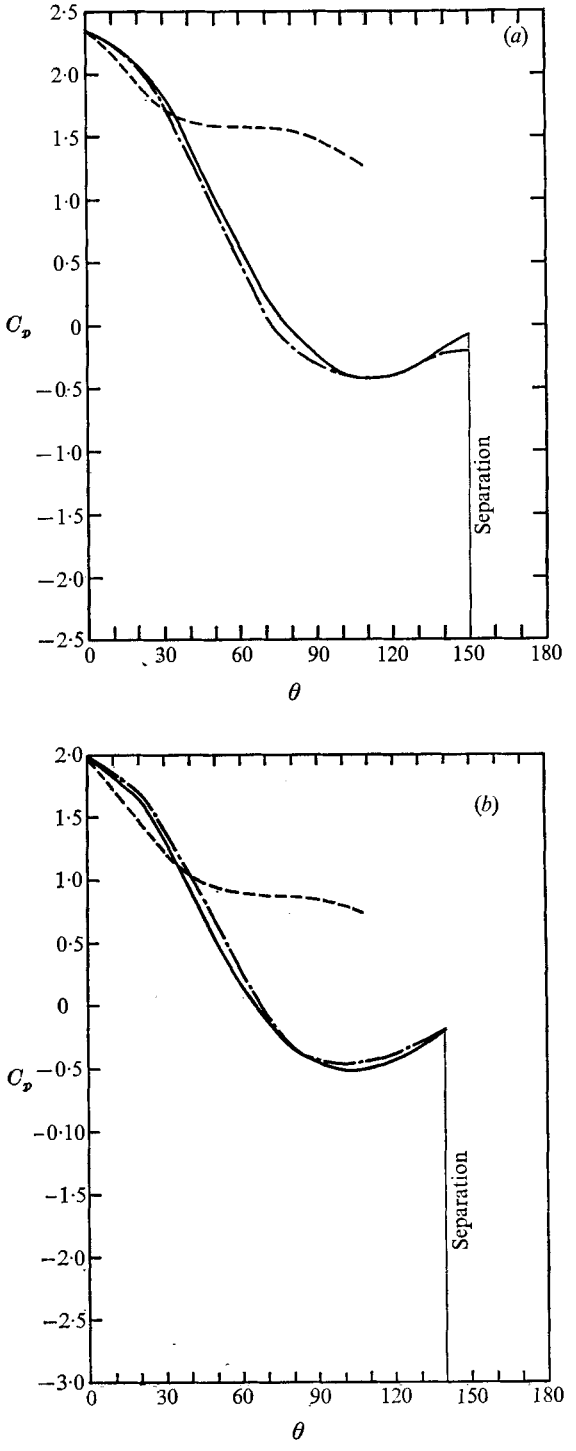

FIGURES 7(*a*, *b*). For legend see next page.

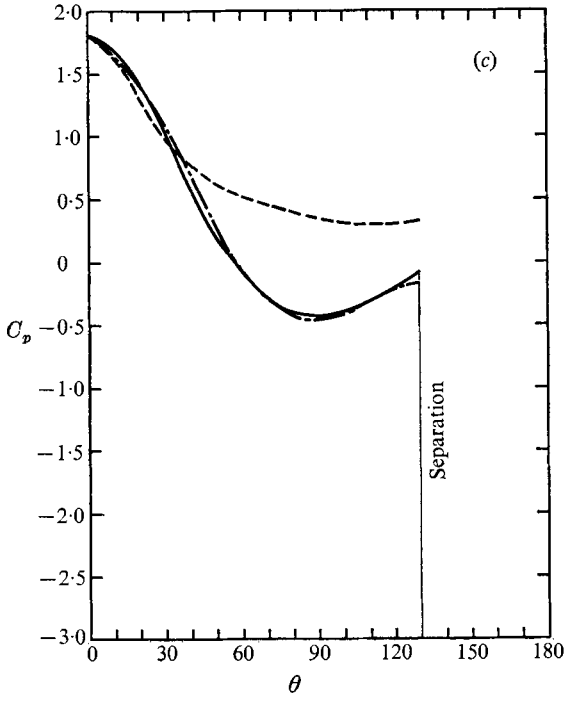

FIGURE 7. Surface pressure distribution around a circular cylinder. ———, second-order approximation; —·—, (*a*, *b*) Kawaguti & Jain (1966), (*c*) Son & Hanratty (1969); – – –, second-order boundary-layer theory. (*a*) $Re_\infty = 10$. (*b*) $Re_\infty = 20$. (*c*) $Re_\infty = 40$.

The dramatic improvement over second-order boundary-layer theory in the prediction of the surface pressure distribution achieved by using the new pressure hypothesis (see figure 7) can be attributed to the greatly improved representation of the first-order displacement body that results from the present solution procedure. In the conventional boundary-layer theory, where the first-order solution for the displacement body is based on the potential flow past the original body surface, separation occurs at approximately 108° from the forward stagnation point regardless of the Reynolds number. In contrast, the stretching of the body co-ordinate implicit in the new pressure hypothesis leads in the first trial solution to a reasonable prediction of the separation-point location as observed in figure 6. The importance of the new pressure hypothesis is clearly demonstrated in figure 8, where we have compared the angular locations of the minimum surface pressure predicted by second-order boundary- layer theory and the present approximate theory respectively with available Navier–Stokes numerical solutions.

Figure 9 shows a typical surface vorticity distribution. As noted in the earlier work of Gluckman (1971) and Werle & Wornom (1972) and mentioned in the introduction, the boundary-layer equations yield reasonable predictions of the surface vorticity distribution provided the surface pressure distribution is accurately known. Figures 10(*a*) and (*b*) show the development of the velocity

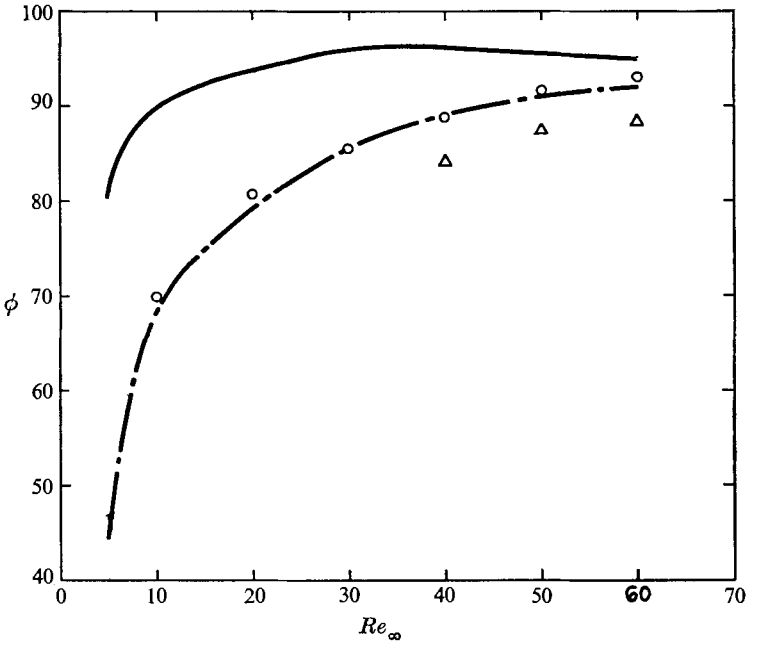

FIGURE 8. Angle of minimum surface pressure for a circular cylinder. —·—, second-order approximation; ———, second-order boundary-layer theory; △, Jain & Rao (1969); ○, Kawaguti & Jain (1966).

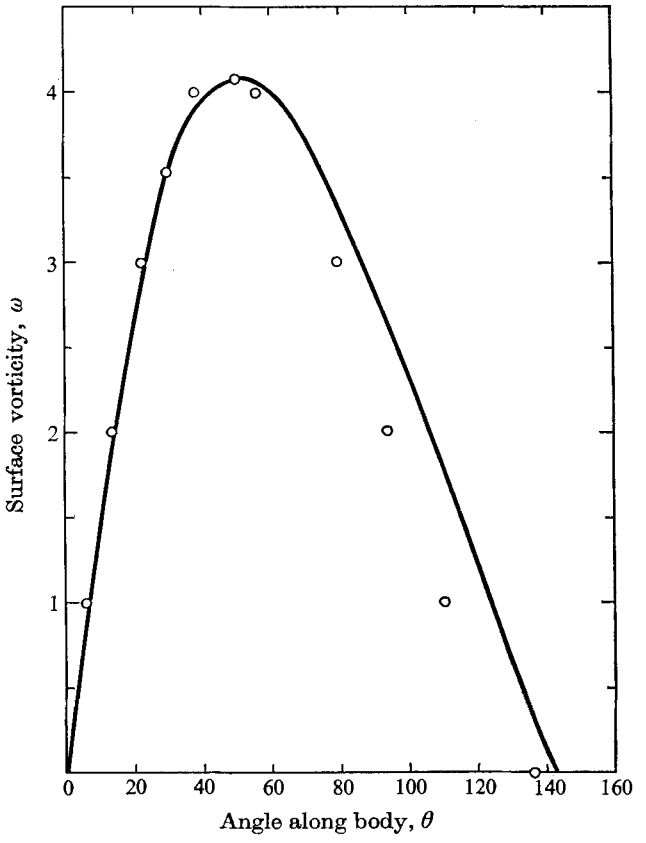

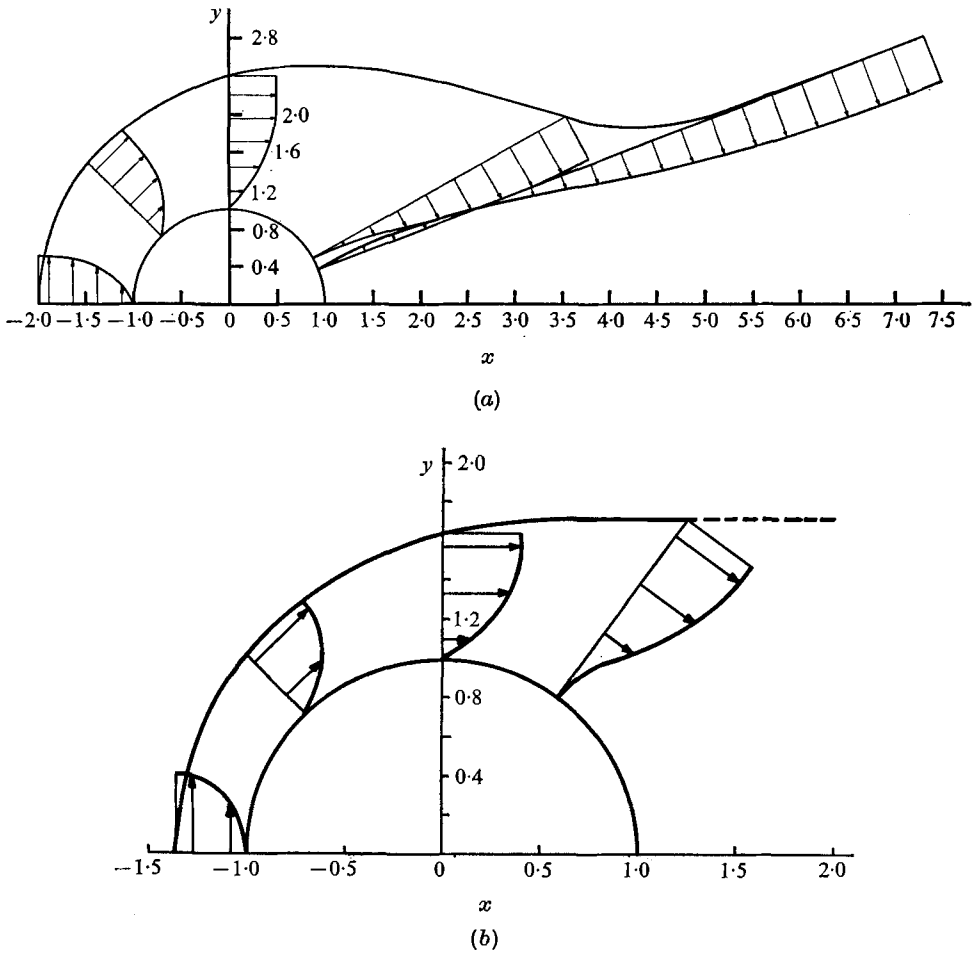

FIGURE 10. Velocity-profile development in the viscous layer around a circular cylinder. (*a*) $Re_\infty = 10$. (*b*) $Re_\infty = 60$.

profile in the viscous layer and the growth of the boundary-layer thickness up to separation at Reynolds numbers of 10 and 60 respectively. Figure 10(*b*) also shows the shape that the fourth-order polynomial profile assumes shortly downstream of separation. No difficulty is encountered in integrating the momentum integral equation (15) through separation using the interaction pressure field. Thus if a more accurate family of separated flow profiles is constructed one should be able to obtain reasonable solutions for the wake separation bubble. This possibility is currently being studied.

7. Additional results and comments

Available published two-dimensional numerical Navier–Stokes solutions have primarily focused on the parabolic- and circular-cylinder geometries already discussed and the conformal family of semi-infinite bodies with a shoulder treated

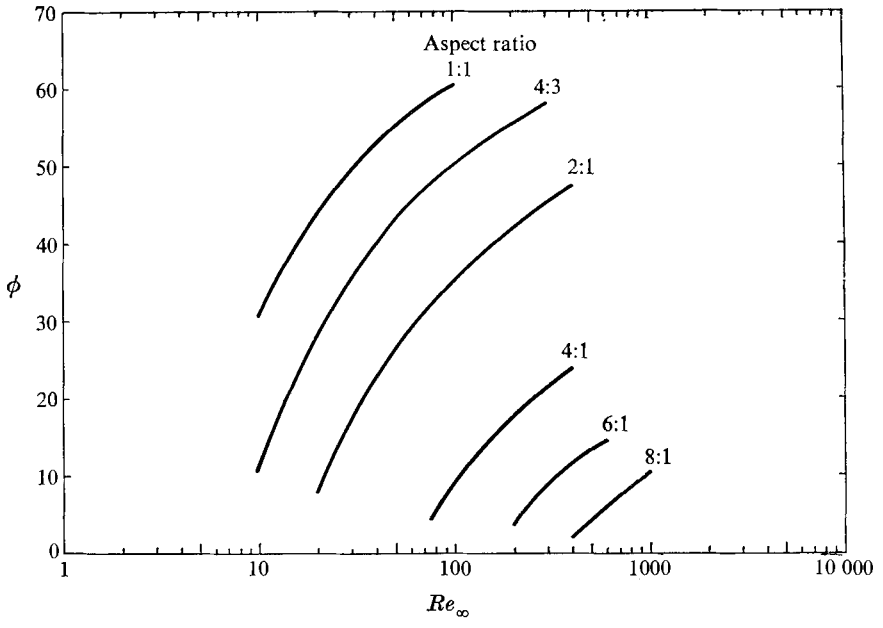

FIGURE 11. Separation angle as a function of Reynolds number for elliptic cylinders, with aspect ratio as a parameter. First-order approximation.

by Davis and co-workers. Based on the derivation presented in § 2, the approximate theory described herein is confined to smoothly contoured bodies whose shoulder radius of curvature does not vary rapidly over a distance comparable to the local boundary-layer displacement thickness. Other, unpublished two-dimensional numerical Navier–Stokes solutions for which the present theory is applicable have been privately communicated to the authors. S. C. R. Dennis has recently examined the Reynolds number for incipient separation on an elliptic cylinder whose aspect ratio (ratio of major to minor axis, the major axis being oriented parallel to the flow direction) is 5·0. The numerical results indicate that the Reynolds number for incipient separation based on the major axis is nearly 200 compared with a value of only 6 for a circular cylinder; see figure 6. This interesting result prompted the authors to undertake a study of the effect of aspect ratio on the angle of separation ϕ for various elliptic cylinders. The angle ϕ is measured from the rear stagnation point to the radius vector from the geometric centre of the body. These results using the new approximate theory are shown in figure 11. Incipient separation for an elliptic cylinder whose aspect ratio is 5·0 occurs according to the present theory at a Reynolds number of approximately 100. While this value appears to differ significantly from that found by Dennis, one observes in figure 11 that the separation angle at a Reynolds number of 200 is still only a few degrees. The wake separation bubble would, therefore, be very small and difficult to detect in any event.

The new pressure hypothesis and approximate theory described herein have also been applied to a variety of semi-infinite and finite axisymmetric three-dimensional bodies; the results are reported in a companion paper (Kolansky

et al. 1977). The agreement with available numerical Navier–Stokes solutions for the flow past paraboloids of revolution and spheres is on a par with that of the two-dimensional results presented herein.

In summary, the proposed approximate theory, which is based on a reasonable intuitive derivation rather than rational arguments, has been shown to be in very good agreement with a broad spectrum of numerical Navier–Stokes solutions for the flow past smoothly contoured bodies in the Reynolds number range 5 to approximately 100. The theory can be easily applied to many boundary shapes for which published numerical Navier–Stokes solutions do not currently exist, e.g. the elliptic cylinders just considered. The important fundamental contribution of the study is the improved understanding of the role and construction of the displacement body and the effect of centrifugal forces in thick viscous layers. Computational times required to obtain a converged solution for most cases shown vary between 1 and 5 seconds on an IBM 360/65 computer.

This research was supported by the Office of Naval Research under contract NR-061-208.

REFERENCES

APELT, C. J. 1961 *Aero. Res. Counc. R. & Mem.* no. 3175.

BRILEY, W. R. & MCDONALD, H. 1974 *United Aircraft Res. Lab. Rep.* no. N110887-3.

CATHERALL, D. & MANGLER, K. W. 1966 *J. Fluid Mech.* **26**, 163.

DAVIS, R. T. 1972 *J. Fluid Mech.* **51**, 417.

DAVIS, R. T. 1974 *Univ. Cincinnati Rep.* no. AFL 74-12-14.

DENNIS, S. C. R. & CHANG, G. 1970 *J. Fluid Mech.* **42**, 471.

GHIA, K. N., GHIA, V. & TESCH, W. A. 1975 *AGARD Symp. Flow Separation, Gottingen, Germany.*

GHIA, V. & DAVIS, R. T. 1974 *A.I.A.A. J.* **12**, 1659.

GLUCKMAN, M. J. 1971 Ph.D. dissertation, The City University of New York.

GROVE, A. S., SHAIR, F. H., PETERSEN, E. E. & ACRIVOS, A. 1963 *J. Fluid Mech.* **19**, 60.

HOMANN, F. 1936 *ForschArb. IngWes.* **7**, 1.

JAIN, P. C. & RAO, K. S. 1969 *Phys. Fluids Suppl.* **2**, II–57.

KAWAGUTI, M. & JAIN, P. 1966 *J. Phys. Soc. Japan*, **21**, 2055.

KOLANSKY, M. S., WEINBAUM, S. & PFEFFER, R. 1976 Submitted to *J. Fluid Mech.*

LIGHTHILL, M. J. 1958 *J. Fluid Mech.* **4**, 383.

MESSITER, A. F. 1970 *SIAM J. Appl. Math.* **18**, 241.

POHLHAUSEN, K. 1921 *Z. angew. Math. Mech.* **50**, 252.

SCHLICHTING, H. 1968 *Boundary-Layer Theory.* McGraw-Hill.

SON, J. S. & HANRATTY, T. J. 1969 *J. Fluid Mech.* **35**, 369.

STEWARTSON, K. 1969 *Mathematika* **16**, 106.

TAKAMI, H. & KELLER, H. B. 1969 *Phys. Fluids Suppl.* **2**, 12.

TANEDA, S. 1956 *J. Phys. Soc. Japan*, **11**, 302.

VAN DYKE, M. 1962 *J. Fluid Mech.* **14**, 161.

WERLE, M. J. & BERNSTEIN, J. M. 1975 *A.I.A.A.* 13 *Aerospace Sciences Mtg., Pasadena, Calif.*, paper 75–8.

WERLE, M. J. & WORMAN, S. F. 1972 *Int. J. Engng Sci.* **10**, 875.